ACS APPLIED BIO MATERIALS Cite This: ACS Appl. Bio Mater. XXXX, XXX, XXX−XXX

Article

www.acsabm.org

Multivalent Supramolecular Self-Assembly between β-Cyclodextrin Derivatives and Polyoxometalate for Photodegradation of Dyes and Antibiotics

Jing Wang, Yong Chen, Ni Cheng, Li Feng, Bo-Han Gu, and Yu Liu*

College of Chemistry, State Key Laboratory of Elemento-Organic Chemistry, Nankai University, Tianjin 300071, P. R. China

Supporting Information

ABSTRACT: An organic−inorganic hybrid supramolecular self-assembly was successfully constructed by multivalent interaction of ethylenediamine-β-cyclodextrin and polyoxometalate in water, which was comprehensively characterized by UV−vis, NMR, Fourier transform infrared spectroscopy, dynamic light scattering, scanning electron microscopy, transmission electron microscopy, Raman spectra, and zeta potential. Interestingly, the resultant nanoparticles exhibited highly efficient catalytic ability for the photodegradation of organic dyes rhodamine B, xylenol orange, methyl orange, methylene blue, and crystal violet, and antibiotics nitrofurazone, tetracyclines, and berberine in the presence of H_2O_2 under the irradiation of mercury lamp or sunlight, which provides ideas for the treatment of organic pollutants.

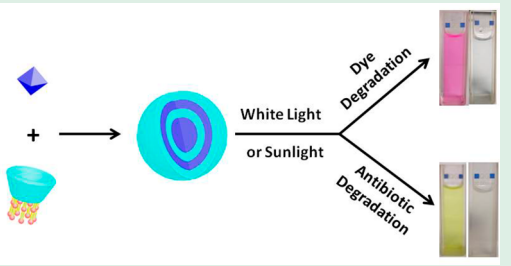

KEYWORDS: *supramolecular assembly, multivalent interaction, dyes, antibiotics, photodegradation*

INTRODUCTION

Since Fujishima et al. published a research paper on hydrogen production from TiO_2 single crystal electrolyzed water in 1972,[1] photocatalytic reactions have attracted the attention of many scholars in the fields of materials,[2] chemistry,[3] physics,[4] environmental protection,[5] etc. Compared with traditional adsorption and concentration filtration methods, photocatalyst has the advantage of simple structure, easily controlled operating condition, strong oxidizing ability, and no secondary pollution.[6] From the various research results, the effect of photocatalysis on the actual pharmaceutical wastewater and printing/dyeing wastewater treatment has been recognized.[7−9] So far, many inorganic semiconductors, alloys, and metal oxides have been widely investigated as photocatalysts, and some of them possessed excellent catalytic reaction capacity.[10] In addition, organic−inorganic hybrid photocatalysts using cucurbit[8]uril and $Na_4SiW_{12}O_{40}$ were also constructed for photocatalytic degradation of dyes.[11]

Polyoxometalates (POMs) are a type of clusters with rich topological structure and properties.[12,13] They are widely concerned nowadays due to their unique advantages such as low toxicity and high degree of mineralization.[14] Among the various POMs, heteropolyacids, a series of POM formed by dehydration between two or more oxoacid salts, are considered to be an environmentally friendly catalyst with mild conditions, stable performance, good synergy, and high photolysis efficiency, and thus have been widely used in the fields of catalysis,[15,16] medicine,[17] biology,[18] energy conversion,[19] and inorganic−organic hybrid materials with novel structures and unique functions.[20,21]

On the other hand, macrocycles with shape-persistent cavities[22,23] are ideal building blocks for the construction of hybrid assemblies[24] because they can encapsulate suitable guests.[25−29] Their excellent inclusion capabilities have led to wide applications in medicine,[30] catalyst,[31] nanotechnology,[32] pharmaceutics,[33−36] and environmental science.[37] Wu et al. reported a new strategy to build free-standing single-layer 2D supramolecular polymer frameworks via synergistic ionic self-assembly of cationic α-cyclodextrin (CD)-based pseudorotaxane bridging sticks with the anionic POM cluster nodes in water.[38] Liu et al. successfully constructed 2D hybrid nanosheets using pillar[6]arenes (P_6) and POM in water, where the macrocyclic cavity of P_6 could impose a restriction effect on the lamellar arrangement and greatly enhance the catalytic ability of nanosheets for dye degradation.[39] Because of the high chemical stability and low biodegradability, dye is regarded as one of the main pollutants in the industrial wastewater such as printing, dyeing, papermaking, and textile.[40] In addition, the frequent occurrence of antibiotics in the water environment has also received increasing public attention.[41] The wastewater produced during the production of antibiotics is the main source of the antibiotic pollution because this wastewater contains a high concentration of antibiotics that can be enriched in plants or aquatic organisms and eventually damage human via the food chain. Recently, green and economic treatment of wastewater from dye and pharmaceutical industry has become a new challenge. There-

Received: September 16, 2019
Accepted: November 5, 2019
Published: November 5, 2019

DOI: 10.1021/acsabm.9b00845
ACS Appl. Bio Mater. XXXX, XXX, XXX−XXX

Scheme 1. Possible Self-Assembly Models of EDA-CD and POM, and Hybrid Nanoparticles, Chemical Formula, and Corresponding Cartoon Representations of EDA-CD and POM[46]

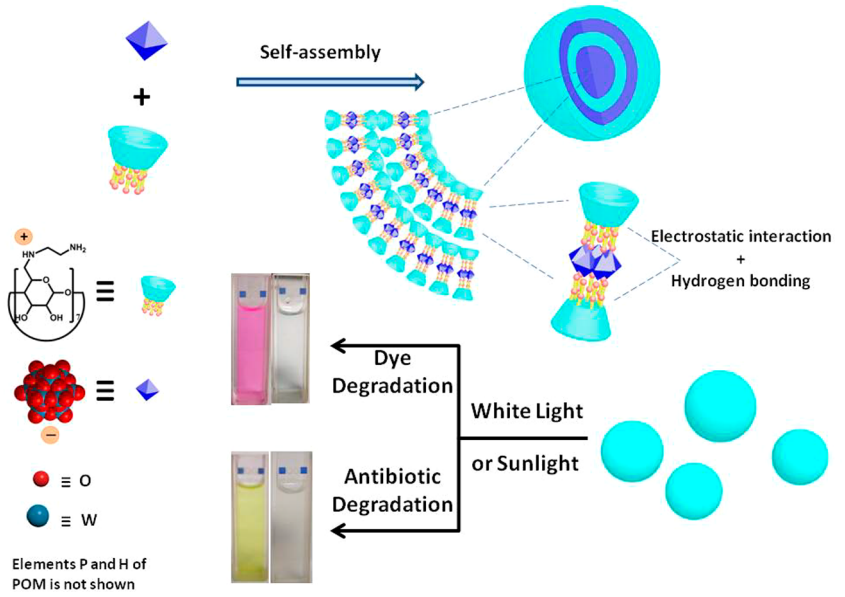

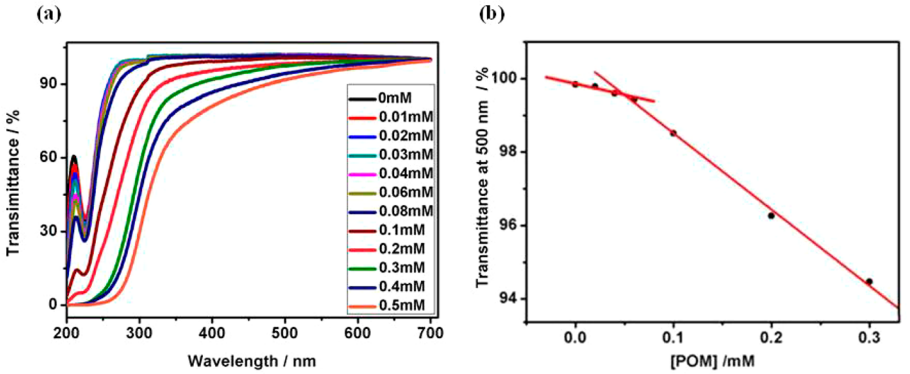

Figure 1. (a) Optical transmittance of POM solutions at different concentrations in the presence of EDA-CD (0.03 mM) at 25 °C. (b) Dependence of optical transmittance at 500 nm on POM concentration in the presence of EDA-CD (0.03 mM).

fore, one can hypothesize that the association of macrocycles and POMs via multivalent interaction may bring a new idea for the treatment of organic wastewater and a breakthrough in supramolecular and material chemistry.

RESULTS AND DISCUSSION

Herein, we constructed a new supramolecular hybrid assembly using phosphotungstic acid ($H_3PW_{12}O_{40}$, here is referred to POM) as polyanionic building blocks and polycationic per-6-deoxy-6-ethylenediamine-β-cyclodextrin (EDA-CD) as polycationic building blocks (Scheme 1). EDA-CD is water-soluble, possesses many amino groups, and can be partially cationized in aqueous solution to generate positive charges,[42] so it is easy to form an assembly with negatively charged POM. The inherent advantages of this supramolecular hybrid assembly are as follows. (1) The electrostatic interactions between polyanionic POMs and polycationic EDA-CDs can promote the formation of assembled nanostructures. (2) β-Cyclodextrin cavity that is formed by seven D-glucopyranose units through the α-1,4-glycosidic bond can encapsulate organic or biological substrates[43−45] and thus enable the close contact of encapsulated substrates with POM catalytic centers. As a result, the EDA-CD/POM hybrid assembly exhibited a highly efficient photodegradation ability toward organic dye and antibiotic in the presence of H_2O_2 under the irradiation of mercury lamp or sunlight.

As a polycationic polymer that has high water solubility, it is difficult for POM to form a self-aggregate independently. However, after the mixing of EDA-CD and POM in aqueous solution, an obvious Tyndall effect was observed, which indicated the formation of large aggregates in solution.[47] In contrast, no Tyndall phenomenon was observed in cases of free EDA-CD or POM (Figure S5, Supporting Information). Figure 1 illustrated the changes of optical transmittance of the EDA-CD aqueous solution (0.03 mM) with the addition of POM. By keeping the concentration of EDA-CD as a constant and changing the concentrations of POM from 0 to 0.5 mM, the optical transmittances at 500 nm exhibited the different linear variation, accompanied by the appearance of an inflection point at 0.055 mM. Thus, the EDA-CD-induced critical aggregation concentration (CAC) value of POM was determined as 0.055 mM. In the contrast, no obvious changes of the optical transmittance could be observed without EDA-

DOI: 10.1021/acsabm.9b00845
ACS Appl. Bio Mater. XXXX, XXX, XXX−XXX

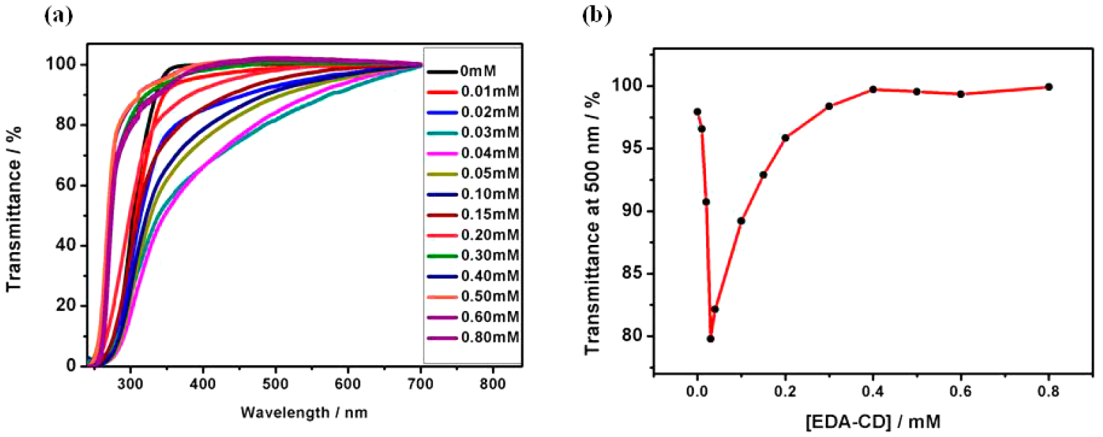

Figure 2. (a) Optical transmittance of POM (0.055 mM) by increasing the concentration of EDA-CD from 0 to 0.8 mM at 25 °C. (b) Dependence of the optical transmittance at 500 nm on EDA-CD concentration in the presence of POM (0.055 mM).

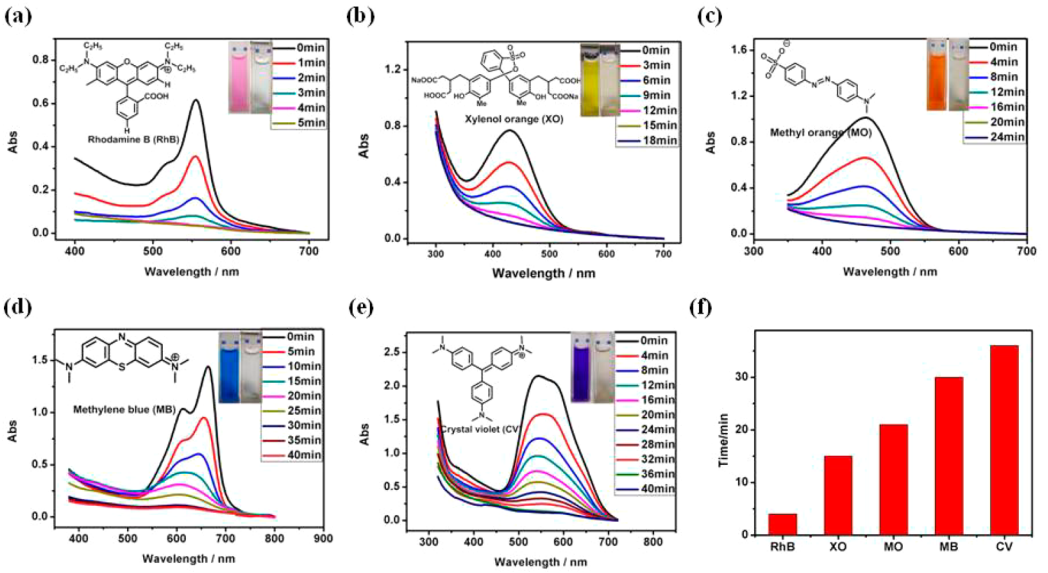

Figure 3. UV−vis spectra of dyes before and after degradation with the EDA-CD/POM hybrid assembly (insert pictures: structures of dyes, photos of solution before and after degradation): (a) RhB, (b) XO, (c) MO, (d) MB, (e) CV. (f) Time dependence of dyes degradation efficiency under the white light irradiation of mercury lamp (50 W).

CD under the same condition (Figure S4, Supporting Information).

By fixing the concentration of POM (0.055 mM) as a constant and gradually increasing the concentration of EDA-CD, the preferable mixing ratio between EDA-CD and POM was determined (Figure 2). As shown in Figure 2b, the optical transmittance of the mixture at 500 nm showed a trend of decreasing rapidly first and then rising to a quasi-plateau. The lowest point was observed at a concentration of EDA-CD at 0.03 mM. The formation of large aggregates may result in the rapid decrease of optical transmittance. With the further addition of EDA-CD, the aggregates would disassemble, and the solution would become clear again. Therefore, 0.055 mM POM/0.03 mM EDA-CD would be the preferable mixing molar ratio of POM/EDA-CD assembly. No obvious changes of the optical transmittance were observed without POM under the same condition (Figure S4, Supporting Information).

Furthermore, dynamic light scattering (DLS), scanning electron microscopy (SEM), Fourier transform infrared (FT-IR) spectroscopy, Raman spectra, and zeta potential experiments were carried out to characterize the structural features of POM/EDA-CD assembly. As seen in Figure S6a, the average hydrodynamic diameter of POM/EDA-CD assembly was ∼228 nm, but no appreciable DLS signals of free EDA-CD or POM were observed. A SEM image of POM/EDA-CD assembly also showed a number of spherical nanoparticles with diameter of ∼100−180 nm, which was a little smaller than the value from DLS results (Figure S6b, Supporting Information), probably because that the aggregation observed in the SEM images was just a drying artifact. In the FT-IR spectra (Figure S9, Supporting Information), the POM powder displayed three main characteristic absorption peaks at 890 cm^{-1} (W−Ob−W), 968 cm^{-1} (W−Od), and 1075 cm^{-1} (P−Oa), demonstrating a Keggin structure of $[PW_{12}O_{40}]$. After association with EDA-CD, the wave numbers of W−Ob−W, W−Od, and W−Oc−W stretches shifted to 888, 948, and 1042 cm^{-1}, respectively, indicating the strong electrostatic interactions between POM and EDA-CD.[48,49] In addition, the appearance of a new band at 734 cm^{-1} also indicated the formation of a

DOI: 10.1021/acsabm.9b00845
ACS Appl. Bio Mater. XXXX, XXX, XXX−XXX

hydrogen bond between the protons on amino and the O atoms of W−Oc−W. Similarly, obvious differences also existed in the Raman spectra of the POM powder and the POM/EDA-CD assembly. The Raman spectrum of POM powder showed three main characteristic vibration bands at 907, 992, and 1009 cm^{-1} assigned to the stretching modes of W−O−W, W=O, and P−O, respectively (Figure S10, Supporting Information), and the band at 907 cm^{-1} shifted to 880 cm^{-1} in the Raman spectrum of the POM/EDA-CD assembly, indicating possible interactions between POM and EDA-CD.[50] These results jointly demonstrated that POM was incorporated with EDA-CD to a hybrid nanostructure, where the Keggin structure of POM still remained.[51] A possible formation mechanism of this nanostructure may be as follows. As shown in Figure S4, the free POM could not form large self-aggregates. With the addition of EDA-CD, various POM/EDA-CD complexes combined with each other to form large layer-by-layer aggregates that subsequently bent to layer-by-layer nanoparticles with alternating shell structures, and these nanoparticles were stabilized mainly by hydrogen bond and electrostatic interactions. In addition, the POM/EDA-CD assembly presented good stability because its optical transmittance, Tyndall effect, and turbidity showed no obvious changes for at least 140 min at room temperature (Figure S8, Supporting Information). The zeta potential of nanoparticles was measured as −12.22 ± 1.83 mV (Figure S7, pH = 4.32, ionic strength = 0.00033 mol/kg, Supporting Information), showing that the POM/EDA-CD assembly was highly anionic. Therefore, we can deduce that the assembly would have the capability of loading cationic substrates.

Herein, the catalytic photodegradation ability of nanoparticles was investigated, where the dyes rhodamine B (RhB), xylenol orange (XO), methyl orange (MO), methylene blue (MB), and crystal violet (CV), and the antibiotics nitrofurazone (NFZ), tetracyclines (TCY), and berberine (BE) were selected as model substrates, and UV−vis spectroscopy as well as mass spectroscopy was used to monitored the degradation process. In a typical example, 100 μL of 1 mM RhB solution was added into the 3 mL of hybrid material (0.055 mM POM/0.03 mM, EDA-CD) solution. After 10 min of stabilization, 50 μL of H_2O_2 was added into the above suspension. As shown in Figure 3, the POM/EDA-CD hybrid exhibited excellent catalytic activity for the photodegradation of RhB. RhB was completely degraded within 4 min under the white light irradiation of mercury lamp (50 W). UV−vis spectra of XO, MO, MB, and CV before and after degradation with the EDA-CD/POM hybrid assembly were shown in Figure 4b, c, d, e, respectively. Figure 4f summarizes the results of time dependence of dyes degradation efficiency under the white light irradiation of mercury lamp (50 W). Furthermore, using the first-order kinetic model, the degradation reaction rate constants (k) and half-lives of RhB, XO, MO, MB, and CV were calculated as 0.868 ± 0.061 min^{-1} (half-life 0.799 ± 0.052 min), 0.214 ± 0.023 min^{-1} (half-life = 3.241 ± 0.313 min), 0.164 ± 0.016 min^{-1} (half-life = 4.219 ± 0.367 min), 0.119 ± 0.002 min^{-1} (half-life = 5.825 ± 0.109 min), and 0.084 ± 0.003 min^{-1} (half-life = 8.252 ± 0.272 min), respectively (Figure S11, Supporting Information). Significantly, EDA-CD/POM hybrid also showed good degradation ability to RhB under sunlight, and RhB was completely degraded within 14 min in the presence of H_2O_2 (Figure S12, Supporting Information). Moreover, when mixing the RhB solution and EDA-CD/POM/H_2O_2 in dark, no degradation phenomenon

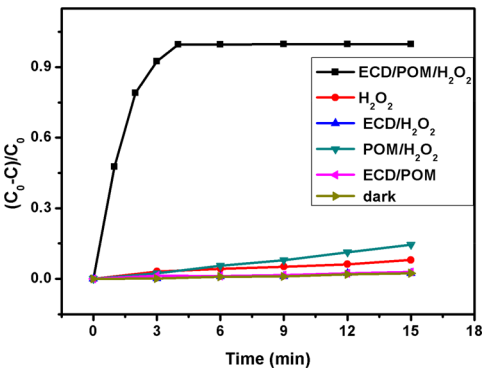

Figure 4. Degradation of RhB over time with different substances or conditions.

was observed, indicating that the light is a key point for the degradation process. In control experiments where the solutions were deareated prior to photocatalytic experiments, the measured degradation reaction rate constants (k) and half-lives of dyes were quite similar to those without deareation (Figure S13, Supporting Information).

To explore the possible mechanism of the degradation reaction, the control experiments by irradiating the mixture of RhB solution with EDA-CD/POM hybrid materials, EDA-CD/H_2O_2, POM/H_2O_2, and H_2O_2 were respectively performed, and the results of the control experiments (Figure 4) showed that these control systems all presented fairly low photodegradation ability toward RhB, and only less than 15% of RhB was degraded within 15 min. Therefore, we deduced that the decrease of RhB concentration in the presence of EDA-CD/POM/H_2O_2 system mainly resulted from the degradation, but not the adsorption of RhB by the EDA-CD/POM hybrid, and the possible mechanism may be as follows. After the mixing of EDA-CD/POM hybrid with H_2O_2 under illumination, $^{\bullet}OH$ was generated, and then $^{\bullet}OH$ degraded RhB to unharmful substances. To confirm this mechanism, isopropanol, a characteristic quencher of $^{\bullet}OH$, was added to the system to investigate the production and contribution of $^{\bullet}OH$ in photocatalytic degradation of RhB. As shown in Figure S14, after the addition of 20 μL of isopropanol, there is almost no significant degradation of RhB. In addition, when using 1-adamantanecarboxylic acid to occupy the cavity of EDA-CD equivalently, the degradation rate was significantly decreased, and only less than 8% of RhB was degraded within 9 min (Figure S15, Supporting Information). Therefore, it can be fully proven that the above-mentioned predicted degradation mechanism is valid.[52] As depicted in Figure S16, during the photocatalytic reaction, catalyst $\{PW_{12}\}$ absorbed light energy to become $^*\{PW_{12}\}$, then $^*\{PW_{12}\}$ captured electrons from water molecules to from $\{PW_{12}\}^-$, and at the same time $^{\bullet}OH$ was generated. In the presence of H_2O_2, $\{PW_{12}\}^-$ was oxidized to $\{PW_{12}\}$ and re-engaged in this process.[53,54] Moreover, the generated $^{\bullet}OH$ was transported to bulk solution easily through the cavity of CD.

More interestingly, the EDA-CD/POM hybrid also presented good photodegradation ability toward antibiotics. Herein, 100 μL of 1 mM NFZ solution was added into the 3 mL solution of hybrid material (0.055 mM POM/0.03 mM, EDA-CD), respectively. After 10 min of stabilization, 50 μL of H_2O_2 was added into the above suspension. As shown in Figure 5a, with the addition of EDA-CD/POM/H_2O_2, almost all of NFZ was degraded within 19 min under the white light

DOI: 10.1021/acsabm.9b00845
ACS Appl. Bio Mater. XXXX, XXX, XXX−XXX

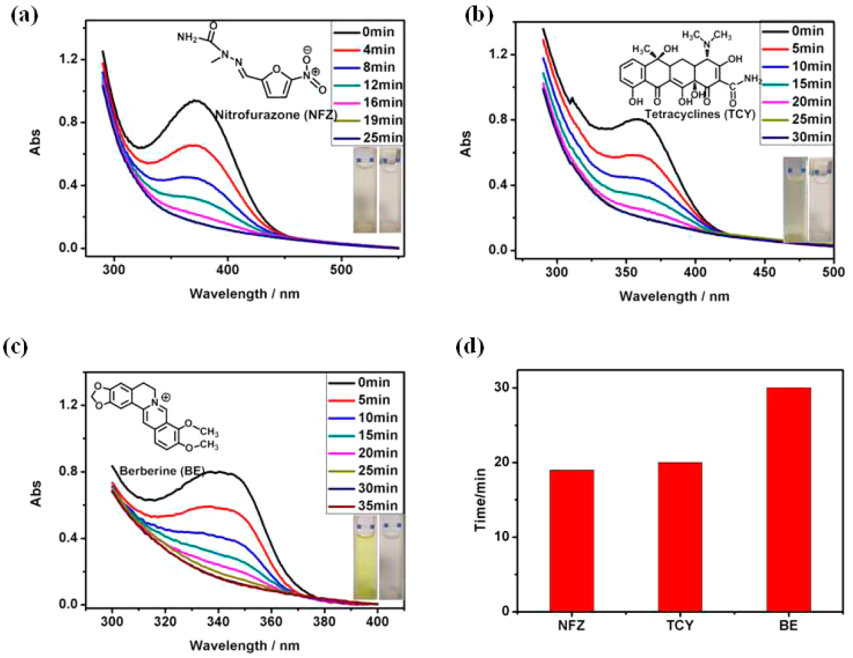

Figure 5. UV−vis spectra of antibiotics before and after degradation with the EDA-CD/POM hybrid assembly (insert pictures: structures of dyes, photos of solution before and after degradation): (a) NFZ, (b) TCY, (c) BE. (d) Time dependence of antibiotics degradation efficiency under the white light irradiation of mercury lamp (50 W).

irradiation of mercury lamp (50 W). UV−vis spectra of TCY and BE before and after degradation with the EDA-CD/POM hybrid assembly were shown in Figure 5b and c, respectively. Figure 5d summarizes the results of time dependence of antibiotics degradation efficiency under the white light irradiation of mercury lamp (50 W). Furthermore, using the first-order kinetic model, the degradation reaction rate constants (k) and half-lives of NFZ, TCY, and BE were calculated as 0.163 ± 0.016 min^{-1} (half-life = 4.258 ± 0.385 min), 0.152 ± 0.016 min^{-1} (half-life = 4.560 ± 0.430 min), and 0.115 ± 0.007 min^{-1} (half-life = 6.024 ± 0.331 min), respectively (Figure S17, Supporting Information).

Compared with previous reports,[39] CD is a readily available natural compound, unlike pillar[6] with aromatic ring, that avoids the introduction of new contaminants. In addition, the main advantages of this work are that the required materials are easier to prepare and can greatly increase the rate of dye degradation as compared with the those reported by Cao[11] and Kaowphong.[55]

CONCLUSION

In summary, we successfully constructed a hybrid nanoparticle through a self-assembly strategy using EDA-CD and POM in water. Rhodamine B (RhB), xylenol orange (XO), methyl orange (MO), methylene blue (MB), and crystal violet (CV), and the antibiotics nitrofurazone (NFZ), tetracyclines (TCY), and berberine (BE) were selected as typical organic pollutants to examine the catalytic activity of the prepared hybrid nanoparticle. The results showed that the nanoparticle exhibited the high catalytic activity for the degradation in the presence of white light and H_2O_2. During this process, $^{\bullet}OH$ was generated and then was transported to bulk solution via the CD cavity. Thereby, the efficiency of degradation was greatly enhanced.

EXPERIMENTAL SECTION

Materials and Methods. β-CD and berberine chloride were purchased from Sigma-Aldrich. $H_3[PW_{12}O_{40}]$ was purchased from Alfa Aesar. Methyl orange (MO) and H_2O_2 were purchased from Sinopharm Chemical Reagent Co., Ltd. All of these were used without further purification.

^1H NMR and ^{13}C NMR spectra were recorded at 298 Kon a Bruker Avance III 500 MHz instrument. UV−vis spectra and the optical transmittance of the aqueous solution were determined in a quartz cell (light path 10 mm) on a Shimadzu UV-3600 spectrophotometer equipped with a PTC-348WI temperature controller. SEM images were recorded on a Hitachi S-3500N scanning electron microscope. The sample for SEM measurements was prepared by dropping the solution onto a coverslip, followed by evaporating the liquid in air. DLS was recorded on a laser light scattering spectrometer (BI-200SM) equipped with a digital correlator (TurboCorr) at 636 nm at a scattering angle of 90°. The sample solution for DLS measurements was prepared by filtering solution through a 800 nm Millipore filter into a clean scintillation vial. Zeta potential was measured by a Zeta PALS + BI-90 instrument (Brookhaven Co. USA). The light irradiation was performed using a mercury lamp (CEL-HXF300 14 V 50 W). The light intensity was around 50 mW cm^{-2}, and the distance was kept at 10 cm.

Synthesis of Per-6-deoxy-6-ethylenediamine-β-cyclodextrin (EDA-CD). Per-(6-deoxy-6-iodo)-β-cyclodextrin (2 g, 1.05 mmol) and 30 mL of ethylenediamine were added to a 100 mL dry round-bottom flask, and the solid was dissolved by stirring under a nitrogen atmosphere, and the temperature was raised to 80 °C for 18 h. A portion of ethylenediamine was removed by rotary evaporation, and the residue was added dropwise to acetone (about 200 mL) with stirring. At this time, a white precipitate appeared. After filtration, a white solid was obtained and dissolved in a small amount of distilled water. In this way, the operation was repeated twice, and finally, the white solid obtained by suction filtration was dried in a vacuum oven for 8 h to obtain a white powdery solid (1.82 g, yield: 91%). ^1H NMR (400 MHz, D_2O, 25 °C, δ, ppm): 5.09 (s, 7H, H1), 3.91 (m, 14H, H3, H5), 3.51−3.61 (m, 14H, H2, H4), 2.71−2.96 (m, 42H, H6, H7, H8); ^{13}C NMR (101 MHz, D_2O, 25 °C): 101.92, 82.68, 73.04, 72.07,

DOI: 10.1021/acsabm.9b00845
ACS Appl. Bio Mater. XXXX, XXX, XXX−XXX

70.49, 50.13, 48.89, 39.55; HRMS: m/z 477.2627 (calcd for $C_{56}H_{115}O_{28}N_{14}^{3+}$, 477.2663).

Preparation of Nanoparticles and Catalytic Applications. In the typical experiment, 14.28 mg of EDA-CD was added to 10 mL of distilled water to obtain 1 mM EDA-CD solution. Then 28.88 mg of POM was added to 10 mL of distilled water to obtain 1 mM POM solution. And 3 mL of desired nanoparticle solution for degradation was prepared by mixing 165 μL of 1 mM EDA-CD solution, 90 μL of 1 mM POM solution, and 2745 μL of distilled water. Then 100 μL of 1 mM dyes solution (or antibiotics solution) was added into 3 mL of fresh nanoparticle solution.

Dyes and antibiotics were chosen as typical organic contaminants to detect the catalytic ability of the prepared nanoparticles. In the typical experiment, 100 μL of 1 mM dyes solution (or antibiotics solution) was added into the 3 mL solution of nanoparticles and stood for 10 min to achieve stability. Then 50 μL of H_2O_2 was added into the above corresponding solution. At given time intervals, the concentrations of the residual dye were determined by monitoring the absorbance at the maximum adsorption.

■ ASSOCIATED CONTENT

Supporting Information

The Supporting Information is available free of charge on the ACS Publications website at DOI: 10.1021/acsabm.9b00845.

More detailed experimental procedures; ^{1}H NMR, ^{13}C NMR spectra; DLS data; SEM images and figures; zeta potential; UV−vis spectra, FTIR spectra, Raman spectra (PDF)

■ AUTHOR INFORMATION

Corresponding Author

*E-mail: yuliu@nankai.edu.cn.

ORCID

Yu Liu: 0000-0001-8723-1896

Notes

The authors declare no competing financial interest.

■ ACKNOWLEDGMENTS

We thank NNSFC (21672113, 21772099, 21861132001, and 21971127) for financial support.

■ REFERENCES

(1) Fujishima, A.; Honda, K. Electrochemical Photolysis of Water at a Semiconductor Electrode. *Nature* **1972**, *238*, 37−38.

(2) Bai, S.; Zhang, N.; Gao, C.; Xiong, Y. Defect engineering in photocatalytic materials. *Nano Energy* **2018**, *53*, 296−336.

(3) Schreck, M.; Niederberger, M. Photocatalytic Gas Phase Reactions. *Chem. Mater.* **2019**, *31*, 597−618.

(4) Serrano, B.; Ortíz, A.; Moreira, J.; de Lasa, H. I. Photocatalytic Thermodynamic Efficiency Factors. Practical Limits in Photocatalytic Reactors. *Ind. Eng. Chem. Res.* **2010**, *49*, 6824−6833.

(5) Obregón, S.; Amor, G.; Vázquez, A. Electrophoretic deposition of photocatalytic materials. *Adv. Colloid Interface Sci.* **2019**, *269*, 236−255.

(6) Kuvarega, A. T.; Krause, R. W. M.; Mamba, B. B. Nitrogen/Palladium-Codoped TiO2 for Efficient Visible Light Photocatalytic Dye Degradation. *J. Phys. Chem. C* **2011**, *115*, 22110−22120.

(7) Li, Q.; Zhao, T.; Li, M.; Li, W.; Yang, B.; Qin, D.; Lv, K.; Wang, X.; Wu, L.; Wu, X.; Sun, J. One-step construction of Pickering emulsion via commercial TiO_2 nanoparticles for photocatalytic dye degradation. *Appl. Catal., B* **2019**, *249*, 1−8.

(8) Chatterjee, D.; Patnam, V. R.; Sikdar, A.; Joshi, P.; Misra, R.; Rao, N. N. Kinetics of the decoloration of reactive dyes over visible light-irradiated TiO_2 semiconductor photocatalyst. *J. Hazard. Mater.* **2008**, *156*, 435−441.

(9) Guo, Y.; Chu, S.; Yan, S.; Wang, Y.; Zou, Z. Developing a polymeric semiconductor photocatalyst with visible light response. *Chem. Commun.* **2010**, *46*, 7325−7327.

(10) Kim, D. H.; Park, H. S.; Kim, S.-J.; Lee, K. S. Characteristics of Ni 8 wt%-doped titanium dioxide photocatalyst synthesized by mechanical alloying. *Catal. Lett.* **2005**, *100*, 49−52.

(11) Lü, J.; Lin, J.-X.; Zhao, X.-L.; Cao, R. Photochromic hybrid materials of cucurbituril and polyoxometalates as photocatalysts under visible light. *Chem. Commun.* **2012**, *48*, 669−671.

(12) Cronin, L.; Müller, A. From serendipity to design of polyoxometalates at the nanoscale, aesthetic beauty and applications. *Chem. Soc. Rev.* **2012**, *41*, 7333−7334.

(13) Peng, Z. Rational Synthesis of Covalently Bonded Organic−Inorganic Hybrids. *Angew. Chem., Int. Ed.* **2004**, *43*, 930−935.

(14) Proust, A.; Matt, B.; Villanneau, R.; Guillemot, G.; Gouzerh, P.; Izzet, G. Functionalization and post-functionalization: a step towards polyoxometalate-based materials. *Chem. Soc. Rev.* **2012**, *41*, 7605−7622.

(15) Raj, G.; Swalus, C.; Guillet, A.; Devillers, M.; Nysten, B.; Gaigneaux, E. M. Supramolecular Organization in Organic−Inorganic Heterogeneous Hybrid Catalysts Formed from Polyoxometalate and Poly(ampholyte) Polymer. *Langmuir* **2013**, *29*, 4388−4395.

(16) Long, D.-L.; Burkholder, E.; Cronin, L. Polyoxometalate clusters, nanostructures and materials: From self assembly to designer materials and devices. *Chem. Soc. Rev.* **2007**, *36*, 105−121.

(17) Kowalewski, B.; Poppe, J.; Demmer, U.; Warkentin, E.; Dierks, T.; Ermler, U.; Schneider, K. Nature's Polyoxometalate Chemistry: X-ray Structure of the Mo Storage Protein Loaded with Discrete Polynuclear Mo−O Clusters. *J. Am. Chem. Soc.* **2012**, *134*, 9768−9774.

(18) Fu, L.; Gao, H.; Yan, M.; Li, S.; Li, X.; Dai, Z.; Liu, S. Polyoxometalate-Based Organic−Inorganic Hybrids as Antitumor Drugs. *Small* **2015**, *11*, 2938−2945.

(19) Sartorel, A.; Bonchio, M.; Campagna, S.; Scandola, F. Tetrametallic molecular catalysts for photochemical water oxidation. *Chem. Soc. Rev.* **2013**, *42*, 2262−2280.

(20) Weingarten, A. S.; Kazantsev, R. V.; Palmer, L. C.; McClendon, M.; Koltonow, A. R.; Samuel, A. P. S.; Kiebala, D. J.; Wasielewski, M. R.; Stupp, S. I. Self-assembling hydrogel scaffolds for photocatalytic hydrogen production. *Nat. Chem.* **2014**, *6*, 964.

(21) Yvon, C.; Surman, A. J.; Hutin, M.; Alex, J.; Smith, B. O.; Long, D.-L.; Cronin, L. Polyoxometalate Clusters Integrated into Peptide Chains and as Inorganic Amino Acids: Solution- and Solid-Phase Approaches. *Angew. Chem., Int. Ed.* **2014**, *53*, 3336−3341.

(22) Cheng, N.; Chen, Y.; Yu, J.; Li, J.-j.; Liu, Y. Photocontrolled Coumarin-diphenylalanine/Cyclodextrin Cross-Linking of 1D Nanofibers to 2D Thin Films. *ACS Appl. Mater. Interfaces* **2018**, *10*, 6810−6814.

(23) Li, J.-J.; Chen, Y.; Yu, J.; Cheng, N.; Liu, Y. A Supramolecular Artificial Light-Harvesting System with an Ultrahigh Antenna Effect. *Adv. Mater.* **2017**, *29*, 1701905.

(24) Fu, H.-G.; Chen, Y.; Yu, Q.; Liu, Y. A tumor-targeting Ru/polysaccharide/protein supramolecular assembly with high photodynamic therapy ability. *Chem. Commun.* **2019**, *55*, 3148−3151.

(25) Wu, Y.; Shi, R.; Wu, Y.-L.; Holcroft, J. M.; Liu, Z.; Frasconi, M.; Wasielewski, M. R.; Li, H.; Stoddart, J. F. Complexation of Polyoxometalates with Cyclodextrins. *J. Am. Chem. Soc.* **2015**, *137*, 4111−4118.

(26) Ramos, A. I.; Braga, T. M.; Silva, P.; Fernandes, J. A.; Ribeiro-Claro, P.; Lopes, M. d. F. S.; Paz, F. A. A.; Braga, S. S. Chloramphenicol·cyclodextrin inclusion compounds: co-dissolution and mechanochemical preparations and antibacterial action. *CrystEngComm* **2013**, *15*, 2822−2834.

(27) Li, P.; Chen, Y.; Liu, Y. Calixarene/pillararene-based supramolecular selective binding and molecular assembly. *Chin. Chem. Lett.* **2019**, *30*, 1190−1197.

(28) Chen, Y.; Huang, F.; Li, Z.-T.; Liu, Y. Controllable macrocyclic supramolecular assemblies in aqueous solution. *Sci. China: Chem.* **2018**, *61*, 979−992.

DOI: 10.1021/acsabm.9b00845
ACS Appl. Bio Mater. XXXX, XXX, XXX−XXX

(29) Li, J.-J.; Zhang, H.-Y.; Zhang, Y.; Zhou, W.-L.; Liu, Y. Room-Temperature Phosphorescence and Reversible White Light Switch Based on a Cyclodextrin Polypseudorotaxane Xerogel. *Adv. Opt. Mater.* **2019**, *7*, 1900589.
(30) Roux, M.; Sternin, E.; Bonnet, V.; Fajolles, C.; Djedaíni-Pilard, F. Dynamic Lipid Lateral Segregation Driven by Lauryl Cyclodextrin Interactions at the Membrane Surface. *Langmuir* **2013**, *29*, 3677−3687.
(31) Zhou, W.-L.; Zhao, X.; Chen, Y.; Liu, Y. Construction and heterogeneous photooxidization reactivity of a cyclodextrin/porphyrin polyrotaxane network. *Org. Chem. Front.* **2019**, *6*, 10−14.
(32) Shi, Y.; Goodisman, J.; Dabrowiak, J. C. Cyclodextrin Capped Gold Nanoparticles as a Delivery Vehicle for a Prodrug of Cisplatin. *Inorg. Chem.* **2013**, *52*, 9418−9426.
(33) Jing, J.; Szarpak-Jankowska, A.; Guillot, R.; Pignot-Paintrand, I.; Picart, C.; Auzély-Velty, R. Cyclodextrin/Paclitaxel Complex in Biodegradable Capsules for Breast Cancer Treatment. *Chem. Mater.* **2013**, *25*, 3867−3873.
(34) Cheng, N.; Chen, Y.; Yu, J.; Li, J.-j.; Liu, Y. Enhanced DNA Binding and Photocleavage Abilities of β-Cyclodextrin Appended Ru(II) Complex through Supramolecular Strategy. *Bioconjugate Chem.* **2018**, *29*, 1829−1833.
(35) Liu, H.; Cai, X.; Chen, J. Mathematical Model for Cyclodextrin Alteration of Bioavailability of Organic Pollutants. *Environ. Sci. Technol.* **2013**, *47*, 5835−5842.
(36) Liu, J.-H.; Wu, X.; Zhang, Y.-M.; Liu, Y. Photocleavable Supramolecular Polysaccharide Nanoparticles for Targeted Drug Release in Cancer Cells. *Asian J. Org. Chem.* **2018**, *7*, 2444−2447.
(37) Zhang, Y.-M.; Zhang, N.-Y.; Xiao, K.; Yu, Q.; Liu, Y. Photo-Controlled Reversible Microtubule Assembly Mediated by Paclitaxel-Modified Cyclodextrin. *Angew. Chem., Int. Ed.* **2018**, *57*, 8649−8653.
(38) Yue, L.; Wang, S.; Zhou, D.; Zhang, H.; Li, B.; Wu, L. Flexible single-layer ionic organic−inorganic frameworks towards precise nano-size separation. *Nat. Commun.* **2016**, *7*, 10742.
(39) Cheng, N.; Chen, Y.; Wu, X.; Liu, Y. 2D organic−inorganic nanosheets via self-assembly of a pillar[6]arene and polyoxometalate for enhanced degradation efficiency. *Chem. Commun.* **2018**, *54*, 6284−6287.
(40) Zhao, Q.; Liu, Y. Macrocycle crosslinked mesoporous polymers for ultrafast separation of organic dyes. *Chem. Commun.* **2018**, *54*, 7362−7365.
(41) Zhang, Y.; Liang, L.; Chen, Y.; Chen, X.-M.; Liu, Y. Construction and efficient dye adsorption of supramolecular hydrogels by cyclodextrin pseudorotaxane and clay. *Soft Matter* **2019**, *15*, 73−77.
(42) Mourtzis, N.; Paravatou, M.; Mavridis, I. M.; Roberts, M. L.; Yannakopoulou, K. Synthesis, Characterization, and Remarkable Biological Properties of Cyclodextrins Bearing Guanidinoalkylamino and Aminoalkylamino Groups on Their Primary Side. *Chem. - Eur. J.* **2008**, *14*, 4188−4200.
(43) Harada, A.; Takashima, Y.; Nakahata, M. Supramolecular Polymeric Materials via Cyclodextrin−Guest Interactions. *Acc. Chem. Res.* **2014**, *47*, 2128−2140.
(44) Harada, A.; Takashima, Y. Macromolecular Recognition and Macroscopic Interactions by Cyclodextrins. *Chem. Rec.* **2013**, *13*, 420−431.
(45) Nakahata, M.; Takashima, Y.; Yamaguchi, H.; Harada, A. Redox-responsive self-healing materials formed from host−guest polymers. *Nat. Commun.* **2011**, *2*, 511.
(46) Legault, C. Y. *CYLview, 1.0b*; Université de Sherbrooke: Sherbrooke, Quebec, Canada, 2009. http://www.cylview.org.
(47) Yan, X.; Zhu, P.; Fei, J.; Li, J. Self-Assembly of Peptide-Inorganic Hybrid Spheres for Adaptive Encapsulation of Guests. *Adv. Mater.* **2010**, *22*, 1283−1287.
(48) Ishiba, K.; Noguchi, T.; Iguchi, H.; Morikawa, M.-a.; Kaneko, K.; Kimizuka, N. Photoresponsive Nanosheets of Polyoxometalates Formed by Controlled Self-Assembly Pathways. *Angew. Chem.* **2017**, *129*, 3020−3024.
(49) Yang, Y.; Zhang, B.; Wang, Y.; Yue, L.; Li, W.; Wu, L. A Photo-driven Polyoxometalate Complex Shuttle and Its Homogeneous Catalysis and Heterogeneous Separation. *J. Am. Chem. Soc.* **2013**, *135*, 14500−14503.
(50) Ma, Z.; Qiu, Y.; Yang, H.; Huang, Y.; Liu, J.; Lu, Y.; Zhang, C.; Hu, P. Effective Synergistic Effect of Dipeptide-Polyoxometalate-Graphene Oxide Ternary Hybrid Materials on Peroxidase-like Mimics with Enhanced Performance. *ACS Appl. Mater. Interfaces* **2015**, *7*, 22036−22045.
(51) Tao, M.; Sun, N.; Li, Y.; Tong, T.; Wielicako, M.; Wang, S.; Wang, X. Heteropolyacids embedded in a lipid bilayer covalently bonded to graphene oxide for the facile one-pot conversion of glycerol to lactic acid. *J. Mater. Chem. A* **2017**, *5*, 8325−8333.
(52) Leng, Y.; Wang, J.; Zhu, D.; Zhang, M.; Zhao, P.; Long, Z.; Huang, J. Polyoxometalate-based amino-functionalized ionic solid catalysts lead to highly efficient heterogeneous epoxidation of alkenes with H_2O_2. *Green Chem.* **2011**, *13*, 1636−1639.
(53) Chen, C.; Zhao, W.; Lei, P.; Zhao, J.; Serpone, N. *Chem. - Eur. J.* **2004**, *10*, 1956.
(54) Kim, S.; Yeo, J.; Choi, W. *Appl. Catal., B* **2008**, *84*, 148.
(55) Chachvalvutikul, A.; Jakmunee, J.; Thongtem, S.; Kittiwachana, S.; Kaowphong, S. Novel FeVO4/$Bi_7O_9I_3$ nanocomposite with enhanced photocatalytic dye degradation and photoelectrochemical properties. *Appl. Surf. Sci.* **2019**, *475*, 175−184.

DOI: 10.1021/acsabm.9b00845
ACS Appl. Bio Mater. XXXX, XXX, XXX−XXX